Lower-stratospheric aerosol measurements in eastward shedding vortices over Japan from the Asian summer monsoon anticyclone during the summer of 2018

Masatomo Fujiwara[1], Tetsu Sakai[2], Koichi Shiraishi[3], Yoichi Inai[4,5], Sergey Khaykin[6], Haosen Xi[7], Takashi Shibata[8], Masato Shiotani[9], and Laura L. Pan[10]

[1] Faculty of Environmental Earth Science, Hokkaido University, Sapporo, 060-0810, Japan
[2] Meteorological Research Institute, Japan Meteorological Agency, Tsukuba, 305-0052, Japan
[3] Faculty of Science, Fukuoka University, Fukuoka, 814-0180, Japan
[4] Graduate School of Science, Tohoku University, Sendai, 980-8578, Japan
[5] Now at Japan Meteorological Agency, Sapporo, 060-0002, Japan
[6] LATMOS/IPSL, UVSQ, Sorbonne Université, CNRS, Guyancourt, 78280, France
[7] Graduate School of Environmental Science, Hokkaido University, Sapporo, 060-0810, Japan
[8] Graduate School of Environmental Studies, Nagoya University, Nagoya, 464-8601, Japan
[9] Research Institute for Sustainable Humanosphere, Kyoto University, Uji, 611-0011, Japan
[10] National Center for Atmospheric Research, Boulder, CO 80301, USA

Correspondence to: Masatomo Fujiwara (fuji@ees.hokudai.ac.jp)

Abstract

Eastward airmass transport from the Asian summer monsoon (ASM) anticyclone in the upper troposphere and lower stratosphere (UTLS) often involves eastward shedding vortices, which can cover most of the Japanese archipelago. We investigated the aerosol characteristics of these vortices by analysing data from two lidar systems in Japan, at Tsukuba (36.1°N, 140.1°E) and Fukuoka (33.55°N, 130.36°E), during the summer of 2018. We observed several events with enhanced particle signals at Tsukuba at 15.5–18 km altitude (at or above the local tropopause) during August–September 2018, with a backscattering ratio of ~1.10 and particle depolarization of ~5% (i.e., not spherical, but more spherical than ice crystals). These particle characteristics may be consistent with those of solid aerosol particles, such as ammonium nitrate. Each event had a timescale of a few days. During the same study period, we also observed similar enhanced particle signals in the lower stratosphere at Fukuoka. The upper troposphere is often covered by cirrus clouds at both lidar sites. Backward trajectory calculations for these sites for days with enhanced particle signals in the lower stratosphere and days without indicate that the former airmasses originated within the ASM anticyclone, and the latter more from edge regions. Reanalysis carbon-monoxide and satellite water-vapour data indicate that eastward shedding vortices were involved in the observed aerosol enhancements. Satellite aerosol data confirm that the period and latitudinal region were free from the direct influence of documented volcanic eruptions and high latitude forest fires. Our results indicate that the Asian Tropopause Aerosol Layer (ATAL) over the ASM

region extends east towards Japan in association with the eastward shedding vortices, and that lidar systems in Japan can detect
35   at least the lower stratospheric portion of the ATAL during periods when the lower stratosphere is undisturbed by volcanic
eruptions and forest fires. The upper tropospheric portion of the ATAL is either depleted by tropospheric processes (convection
and wet scavenging) during eastward transport or is obscured by much stronger cirrus cloud signals.

1 Introduction

The Asian Summer Monsoon (ASM) circulation includes a continental-scale anticyclone centred over the Tibetan Plateau,
40   spanning from the Middle East to East Asia in the upper troposphere and lower stratosphere (UTLS). Satellite observations
show elevated levels of trace gases of surface origin (e.g., Randel et al., 2010; Santee et al., 2017), aerosol particles (Vernier
et al., 2015, 2018), and water vapour (Randel et al., 2015; Santee et al., 2017) within the ASM anticyclone due to active
convection in this region and season. The ASM anticyclone exhibits distinct sub-seasonal variability due to westward and
eastward shedding vortices (e.g., Popovic and Plumb, 2001; Amemiya and Sato, 2018), with the latter possibly being
45   dynamically linked to the Bonin (or Ogasawara) High in the western Pacific (Enomoto et al., 2003) and constituting a major
transport pathway of ASM airmasses to the whole Northern Hemisphere (NH) midlatitude UTLS through the westerly jet
stream (e.g., Vogel et al., 2014, 2016; Ungermann et al., 2016; Pan et al., 2016; Fadnavis et al., 2018; Luo et al., 2018;
Honomichl and Pan, 2020). Eastward shedding vortex events occur once in every 10–20 days during the NH summer, with a
horizontal scale of 20°–30° longitude (2000–3000 km), and with a few days to one week of influence over the Japanese
50   archipelago (e.g., Honomichl and Pan, 2020).

The enhanced aerosol particle signature in the ASM anticyclone at 14–18 km altitude is known as the Asian Tropopause
Aerosol Layer (ATAL), which was believed to consist of carbonaceous and sulphate materials, mineral dust, and nitrate
particles (Vernier et al., 2015, 2018; Brunamonti et al., 2018; Bossolasco et al., 2020; Hanumanthu et al., 2020). Through
55   analysis of satellite and high-altitude aircraft observations and laboratory experiments, Höpfner et al. (2019) provided evidence
that a considerable part of the ATAL may contain solid ammonium nitrate (NH_4NO_3) particles. Their satellite data analyses
indicate enhanced NH_4NO_3 signals around the tropopause, both in the ASM region and the western Pacific (including Japan)
during 8–16 August 1997 (with the western Pacific signals suggestive of shedding vortices), with the mass of NH_4NO_3 in the
ASM region at 13–17 km peaking around August. It is also noted that Vernier et al. (2015, in their Figure 2b) showed mean
60   eastward extension of the ATAL to the Japanese archipelago by averaging Cloud–Aerosol Lidar with Orthogonal Polarization
(CALIOP) data for July–August 2006–2013, although the role of synoptic disturbances, such as eastward shedding vortices,
in the ATAL eastward extension does not appear to have been investigated using CALIOP data.

Some lidar systems currently in operation in Japan are capable of measuring UTLS aerosol characteristics, including those at
65   the Meteorological Research Institute (MRI), Tsukuba (36.1°N, 140.1°E; Sakai et al., 2016) and Fukuoka University, Fukuoka

(33.55°N, 130.36°E; Yasui et al., 1995). Both systems measure the backscattering ratio (BSR; related to particle size and density) and particle depolarization ratio (PDR; related to the degree of particle non-sphericity). Previous studies using data from these systems investigated the impacts of the large-scale tropical volcanic eruptions and other recent eruptions (Uchino et al. 1993; Sakai et al. 2016), and spring-time transport of dust particles from the Asian continent, "Kosa" events (yellow

70   sand/dust events) (Sakai et al. 2003), amongst others; however, data have not been investigated extensively for the possible detection of the ATAL from ASM circulation, partly because extensive summer-time cloud cover often prevents lidar sensing of the UTLS region, and partly because ATAL signals are much weaker than volcanic signals. In this paper, focusing on the July–September 2018 period, we investigate whether these lidars are capable of measuring ATAL signals associated with eastward shedding vortices from the ASM anticyclone, with combined analyses of backward trajectories, chemical reanalysis

75   data, and satellite data for full understanding of the lidar observations. The remainder of this paper is organised as follows. Section 2 describes the lidar and other data analysed in this paper. Section 3 presents the results and discussion, and Section 4 concludes the findings.

2 Data description

80   ### 2.1 Lidar data

The lidar system at the MRI, Tsukuba (36.1°N, 140.1°E) used in this study is an Nd:YAG system operated at a wavelength of 532 nm, with a capability of both BSR and PDR measurements (Sakai et al., 2016), and which has been operating continuously since 2002. We define PDR as S/P, where S and P are the background-subtracted lidar photon counts of the perpendicular (senkrecht in German) and parallel components, respectively, with respect to the polarization plane of the emitted laser light.

85   The temporal and height resolutions of the original processed data are 5 min and 7.5 m, respectively. Quality control has been made primarily to flag data points influenced by thick cloud layers. To obtain vertical profiles of BSR and PDR with high signal-to-noise ratios, data were averaged over 150 m and 3 h, with time intervals of 18–21, 21–00, 00–03, and 03–06 local time (LT) for the use in this paper. BSR data were normalised to unity at the 30–33 km altitude where aerosol backscattering is assumed to be negligible, and PDR values were obtained using the method of Adachi et al. (2001).

90

The lidar system at Fukuoka (33.55°N, 130.36°E) used in this study is also an Nd:YAG system operated at a wavelength of 532 nm, with PDR measurement capability. This system has been operated manually only during nights under clear-sky/non-rainy conditions; during July–September 2018, the system was operated on 11 nights. Vertical profiles were averaged over 900 m and 4 h for each night for the use in this paper. The PDR for Fukuoka is originally defined as $S/(P+S)$, which has been

95   converted to S/P for this paper.

The uncertainties of lidar data are discussed here, which are applied to the both systems. The BSR uncertainties were estimated from the photon counts of the backscatter signals at 532 nm by assuming Poisson statistics to be 2–3 % typically around the tropopause. The PDR uncertainties were estimated from the parallel and perpendicular components of backscatter signals at

100 532 nm. Other sources of PDR uncertainty (bias) include (1) the uncertainty in calibration of the total depolarization ratio (TDR), due to both particles and air molecules, and (2) the BSR uncertainty. Uncertainty (1) was estimated as follows. In the TDR calibration (Adachi et al., 2001), we subtracted depolarization caused by the lidar system (DEPsys) estimated from the observed TDR and BSR obtained in the altitude region where aerosol backscattering is negligible (i.e., BSR equals unity, and TDR equals the molecular depolarization ratio), or where spherical particles predominate (i.e., in lower tropospheric water

105 clouds). DEPsys errors result in PDR bias. For example, a DEPsys error of ±0.2% results in a ±2% bias in PDR where BSR = 1.1. Uncertainty (2) arises mainly from our assumption that aerosol backscattering is negligible at 30–33 km altitude. We also assumed an aerosol extinction-to-backscatter ratio of 50 sr over the whole measurement height range. These assumptions result in errors in BSR and thus PDR. For example, BSR errors of +0.05 and –0.05 result in a bias of –1% and +3% in PDR, respectively, where BSR = 1.1 and TDR = 0.7%. Based on these considerations, we estimate that the total PDR uncertainty

110 (random plus bias errors) is $\leq\pm5\%$ PDR.

2.2 Other data

Backward trajectories are calculated using the trajectory model used by Inai (2018) and Inai et al. (2018) and the most recent global atmospheric reanalysis dataset by the European Centre for Medium-Range Weather Forecasts (ECMWF), ERA5

115 (Hersbach et al., 2020), with 37 pressure levels up to 1 hPa and horizontal and temporal resolutions of 0.25° × 0.25° and 1 h, respectively.

The Copernicus Atmosphere Monitoring Service (CAMS) atmospheric-composition reanalysis dataset produced by the ECMWF (Inness et al., 2019) is used to analyse signatures of the ASM anticyclone and its eastward shedding vortices, with

120 25 pressure levels up to 1 hPa and horizontal and temporal resolutions of 0.75° × 0.75° and 3 h, respectively. Carbon monoxide (CO), temperature, and potential vorticity data are analysed in this paper. CO is chosen because it is a good tracer for polluted air of surface origin (e.g., Luo et al., 2018). CO data on pressure levels are projected on to isentropic surfaces using temperature data. In the CAMS, the Measurement of Pollution in the Troposphere (MOPITT) thermal infrared (TIR) satellite total-column CO data are assimilated, but, Microwave Limb Sounder (MLS) and Infrared Atmospheric Sounding Interferometer (IASI) CO

125 data are not. The CAMS dataset also includes different types of aerosol particles, but they are not included in this study because relevant variables such as aerosol BSR and NH_4NO_3 concentration are not included. PV projected on to isentropic surfaces calculated from CAMS data are also analysed because it is often used as a dynamical tracer (e.g., Popovic and Plumb, 2001; Amemiya and Sato, 2018). In addition, MLS Version 4.2 Level 2 water-vapour data (Santee et al., 2017; Livesey et al., 2020) are analysed because water vapour is also a good tracer of the ASM anticyclone.

130   The possible influence of volcanic eruptions and wildfire events is investigated using two satellite aerosol-particle datasets, one providing vertical extinction profile data at 675 nm from the Ozone Mapping and Profiler Suite (OMPS) Limb Profiler (LP), Level 2 Version 1.5 (Chen et al., 2018), and the other attenuated scattering-ratio data from the CALIOP onboard the Cloud–Aerosol Lidar and Infrared Pathfinder Satellite Observation (CALIPSO) satellite (Thomason et al., 2007; Winker et al.,

135   2007, 2010). CALIOP Level 3 monthly-mean stratospheric aerosol data (CAL_LID_L3_Stratospheric_APro-Standard-V1-00) are used in this study; in this data product, clouds and Polar Stratospheric Clouds (PSCs) have been removed (Young and Vaughan, 2009; https://www-calipso.larc.nasa.gov/resources/calipso_users_guide/data_summaries/l3/lid_l3_stratospheric_apro_v1-00_v01_desc.php).

3 Results and discussion

3.1 Lidar measurements

    Time–height distributions of BSR and PDR observed in the UTLS at Tsukuba are shown in Figure 1, and the corresponding vertical profiles are shown in Figure 2. Because the PDR has more missing data points, the TDR time–height distribution is also shown in Figure A1. Days that are missing data (white regions; Fig. 1) are due to thick summer-time rain clouds in the

145   lower-to-middle troposphere, which prevented the laser light reaching the middle stratosphere. However, some events with enhanced particle signals are evident just above the tropopause at 15.5–18 km, and last for a few days, mainly in August, but with some in September. In particular, the event peaking at around 21 August and spanning 18–26 August was the strongest one among those the lidar successfully measured during the three-month period. Fig. 2 shows that enhanced particle signals at 15.5–18 km were often observed in August, sometimes in September, but not in July. Typical BSR and PDR values of

150   enhanced signals are ~1.10 (1.07–1.18) and ~5% (3%–10%), respectively (Figs. 1 and 2). Below the tropopause, strong signals were sometimes recorded with BSR values of >1.25 and with PDR values >>10%. In general, the PDR values are 0% for spherical particles (i.e., water clouds in the troposphere and liquid H_2SO_4 particles in the stratosphere) and are >25%–30% for ice cirrus particles (e.g., Sakai et al., 2003; Fujiwara et al., 2009). Strong signals in the upper troposphere are thus due to ice cirrus clouds. Enhanced signals in the lower stratosphere (15.5–18 km) may be due to solid particles, as indicated

155   by the PDR values of ~5% (3%–10%). Taking PDR uncertainties (Sect. 2.1) into account, these values can be considered as small, but non-zero, values. The PDR values of these signals, together with the region being above the local tropopause in most cases, strongly suggest that they are not ice cirrus particles. However, the possibility of mixture of spherical H_2SO_4 particles (i.e., background stratospheric sulphate particles) and highly non-spherical particles, such as ice, volcanic ash (Prata et al., 2017), and wildfire smoke (Haarig et al., 2018), cannot be precluded only with our lidar data. We will come back to

160   this issue in Sect. 4 after investigating several other data.
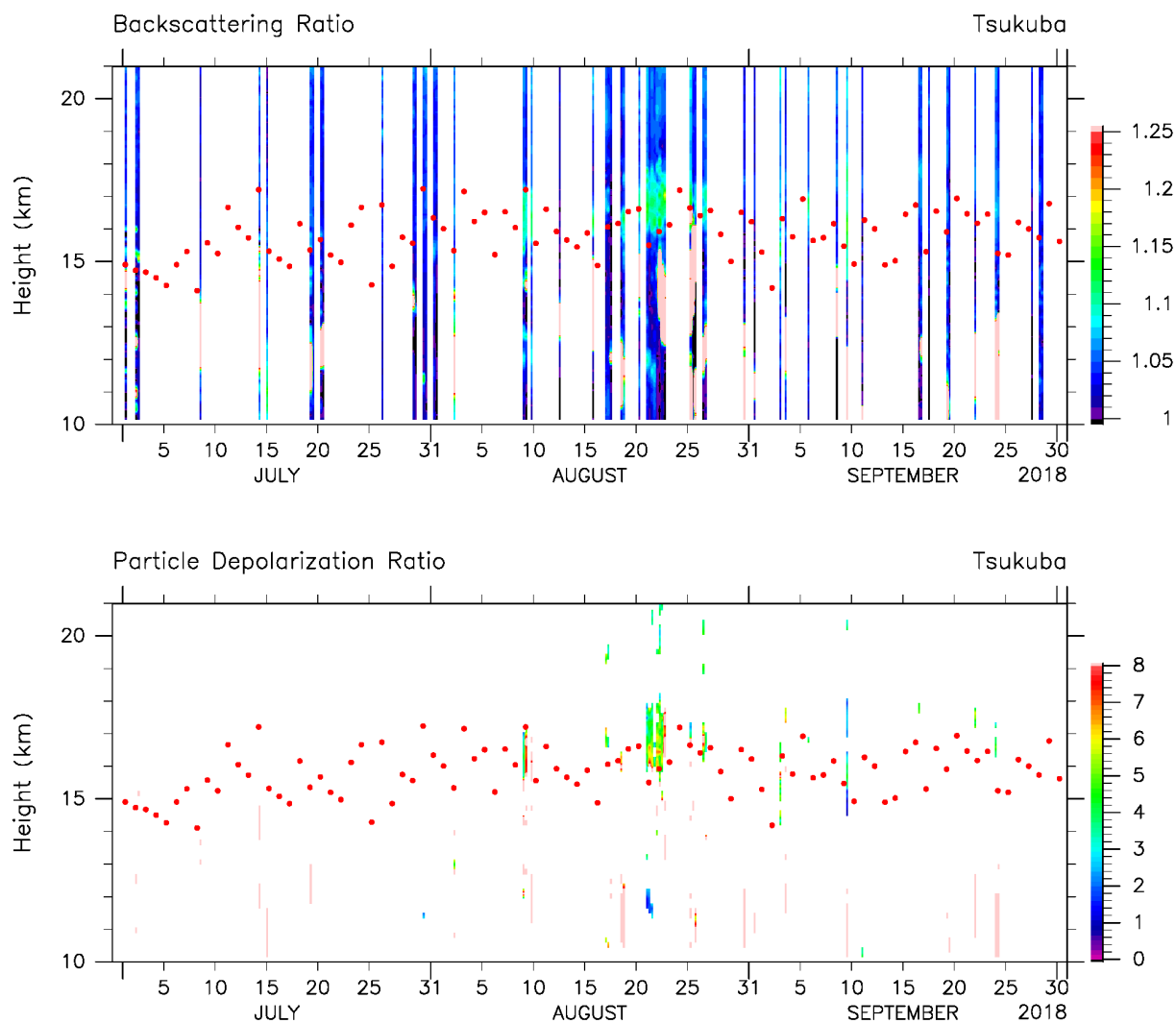
Figure 1 Time–height distributions of (top) backscattering ratio and (bottom) particle depolarization ratio (%) during July–September 2018, as measured using the lidar system at MRI, Tsukuba. For each day, four time slots (i.e., 18–21, 21–00, 00–03, and 03–06 LT) are prepared, with 3-h averaged data filling the slots where thick lower-to-middle tropospheric clouds do not exist. Red dots indicate the daily (first) lapse-rate tropopause locations determined by the Japan Meteorological Agency (JMA), based on 21 LT radiosonde data taken at the JMA "Tateno" site (which shares the same site as the MRI).
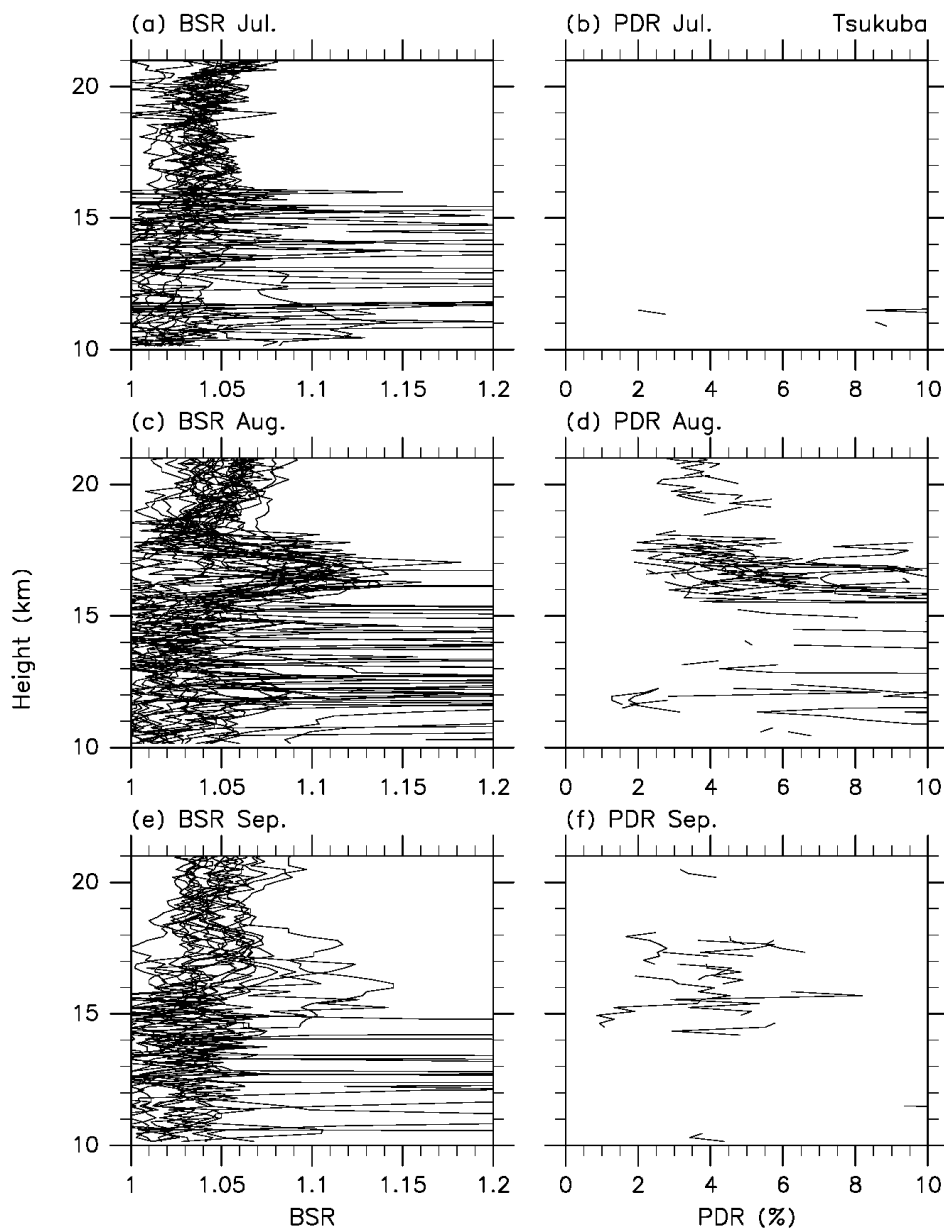
Figure 2 Vertical profiles of (a, c, e) backscattering ratio (BSR) and (b, d, f) particle depolarization ratio (PDR, in %) in (a, b) July, (c, d)
175   August, and (e, f) September 2018 obtained using the lidar system at MRI, Tsukuba. It is noted that strong and noisy signals in BSR below
~15.5 km are due to cirrus clouds.

Vertical profiles of BSR and PDR observed at Fukuoka for 11 clear-sky/non-rainy nights during July–September 2018, are

180   shown in Figure 3. Again, enhanced particle signals were observed mainly in August above the tropopause at 15.5–18 km. The

BSR values were in the range 1.09–1.14, with PDR values of 1%–3% which are smaller than those observed at Tsukuba. It

should be noted that the dates of lidar operation at Fukuoka did not overlap those at Tsukuba when strong enhancement was

observed above the tropopause (e.g., 9 August, 18–26 August, and 9 September), perhaps partly explaining the differences

between Figs. 2 and 3.

185
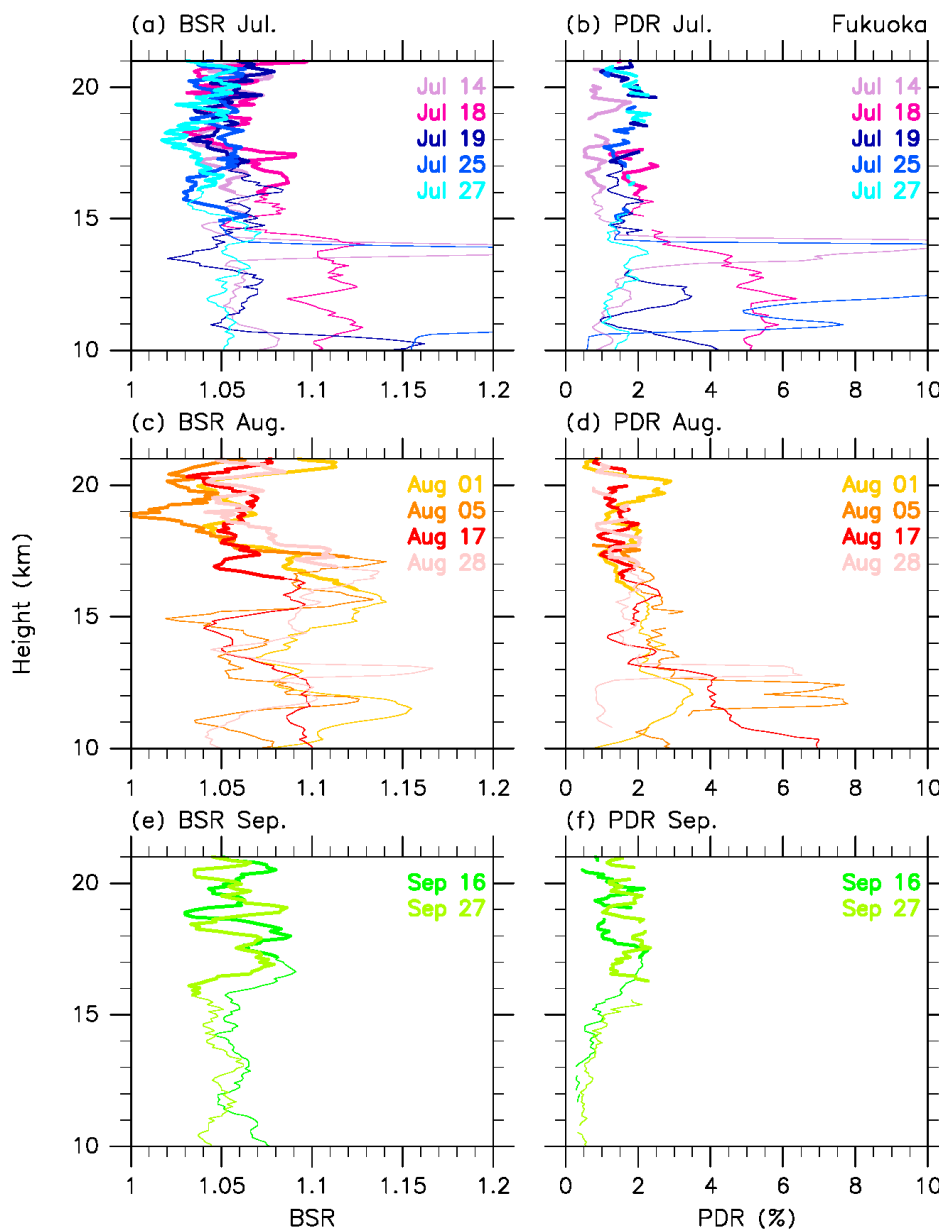
Figure 3 Eleven vertical profiles of (a, c, e) backscattering ratio (BSR) and (b, d, f) particle depolarization ratio (PDR, in %) in (a, b) July,

190 (c, d) August, and (e, f) September 2018 obtained using the lidar system at Fukuoka. Dates and colours are assigned in the legend where,

for example, "Jul 14" refers to the night of July 14–15. Stratospheric portion of the profiles has been thickened using the (first) tropopause

location information provided by the JMA, based on operational 21 LT radiosonde data taken at the JMA Fukuoka site (with a ~4 km

distance from the lidar site).

195

3.2 Trajectories and airmasses

Ten-day kinematic backward trajectories (using vertical wind) from Tsukuba and Fukuoka are shown in Figures 4 and 5, respectively, with contrasting cases with or without aerosol particle enhancement in the 390–410 K potential-temperature range (around 16.5–17.5 km at these stations). The 65 ppbv contours of monthly mean CAMS CO data at a 400 K potential

200 temperature are shown as an index of boundaries of the ASM anticyclone (i.e., within the anticyclone, CO concentration is >65 ppbv). These trajectories indicate that airmasses over both stations come mainly from the west, and sometimes via the north of Japan (indicative of the existence of vortices), and originated from the ASM anticyclone well within 10 days. They also indicate that airmasses with enhanced aerosol particles at this height tend to originate in regions within the ASM anticyclone, whereas those without enhanced aerosol particles tend to originate from edge regions surrounding the anticyclone.

205
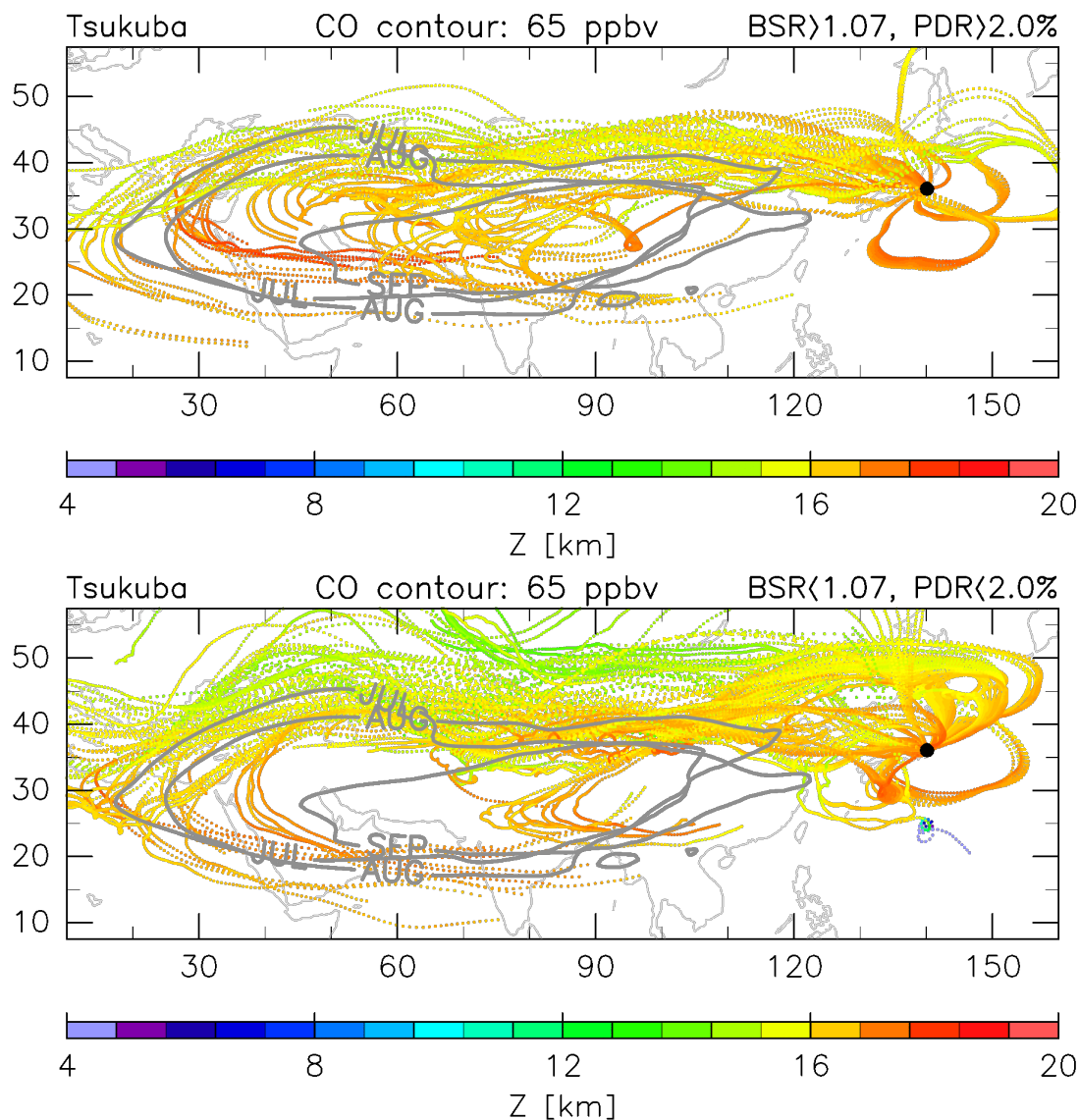
Figure 4 Kinematic backward trajectories for 10 days starting from Tsukuba in the 390–410 K potential temperature range at 100 m
geopotential height intervals during July–September 2018, using ERA5 reanalysis data. Cases are sorted into two categories: (top) with and
(bottom) without enhanced aerosol signals observed by lidar at the trajectory starting points. The conditions and number of trajectories for
the former and the latter cases are, respectively, BSR > 1.07; PDR > 2.0%; 78 trajectories and BSR < 1.07; PDR <2.0%; 136 trajectories.
Colours indicate geopotential height (Z) values of the trajectories. Grey contours indicate 65 ppbv monthly mean CAMS CO levels at 400
K potential temperature, roughly indicating monthly mean boundaries of the ASM anticyclone.
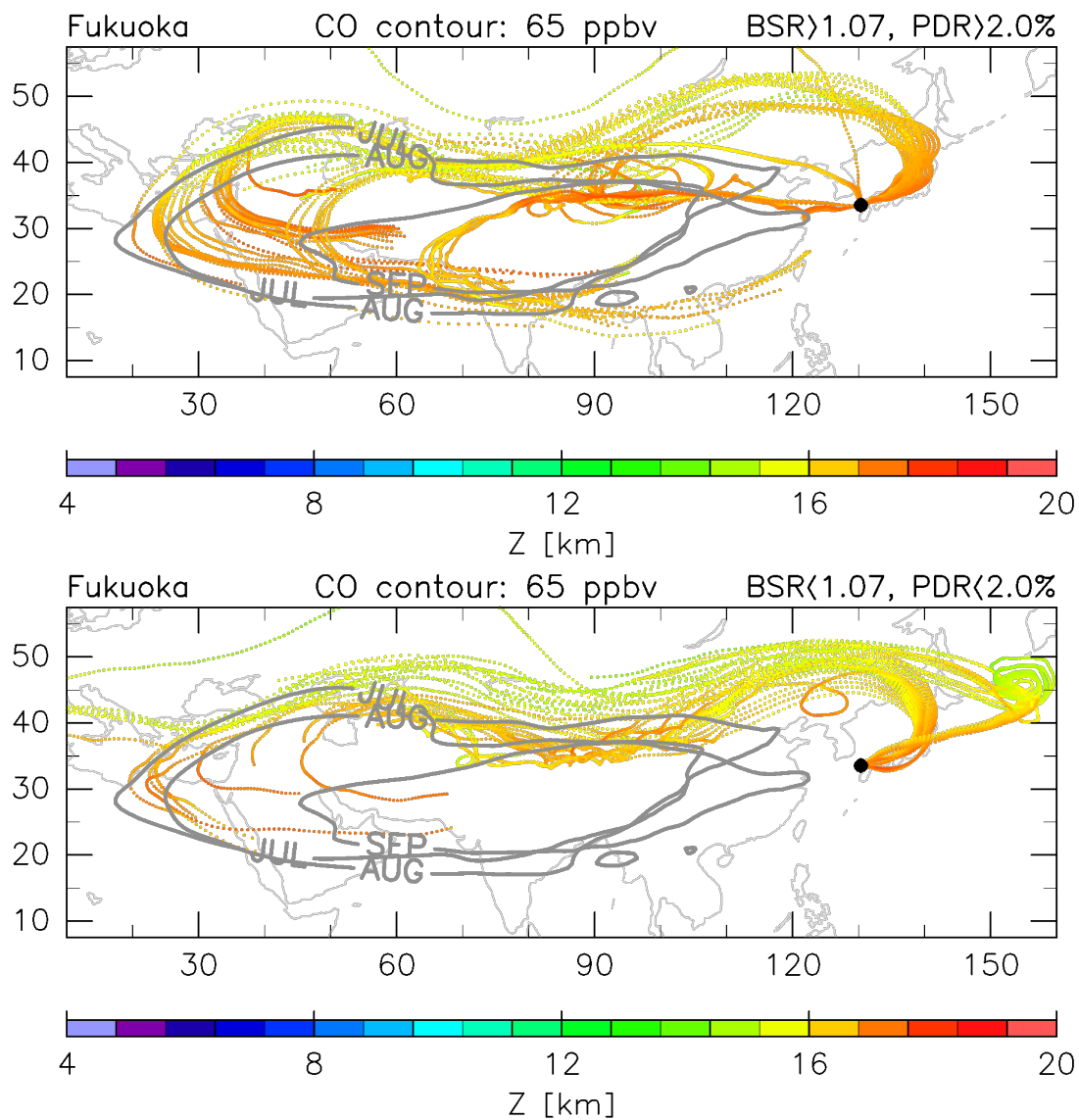
Figure 5 As for Fig. 4, but for trajectories from Fukuoka, with (top) 44 and (bottom) 37 trajectories.

Horizontal distributions of CO and PV at the 400 K potential-temperature surface during 18–23 August 2018 are shown in Figure 6. A potential temperature of 400 K corresponds to altitudes of ~17.1 km at Tsukuba and ~17.3 km at Fukuoka, on average, during July–September 2018 (based on twice-daily radiosonde data at each site, taken from http://weather.uwyo.edu/upperair/sounding.html), i.e., near the centre of the lower stratospheric BSR enhancement. The strongest particle signals during the three months were observed on 21 August in the lower stratosphere over Tsukuba. The airmass with high CO concentrations was transported eastward from the ASM anticyclone centred over the Tibetan Plateau (Fig. 6), with an anticyclonic vortex of ~20° longitude scale reaching the Japanese archipelago on 21 August, providing a clear signature of eastward shedding vortices from the ASM anticyclone (e.g., Luo et al., 2018). PV can be regarded as a dynamical tracer, with lower values in the ASM anticyclone along the same latitudes (e.g., 30°N), although background positive gradients in latitude and its noisier nature give more complicated features. Daily averaged longitude–time CO distributions over 30°N–40°N are shown in Figure 7, with that latitude band chosen here because it includes the two lidar sites. The ASM anticyclone spans roughly 15°N–40°N, whereas the eastward shedding vortices are often located slightly to the north, at around 25°N–45°N, as indicated in Figs. 4–6; the latitude band must therefore be chosen carefully, depending on the research focus. The 60-ppbv CO contour may be a good indicator of eastward shedding vortices (Fig. 7). In July 2018, the eastward extension was weak, but in August there were three events that directly affected the two lidar sites, at August 5–15, 20–25 (Fig. 6) and 27–31. In September, there were three events, at September 3–8, 14–19 and 27–30. A comparison with Fig. 1 indicates that aerosol-particle enhanced events correspond relatively well to CO-enhanced events, although missing lidar data points (due to low-level clouds) result in the fact that only the August 20–25 event was relatively well observed. The ASM anticyclone is also characterised as an airmass hydrated by active convection from below (e.g., Santee et al., 2017). The longitude–time distribution of water vapour at 400 K, averaged over 30°N–40°N with 8°-longitude and 3-day bins, is shown in Figure 8. The water-vapour-enhanced events over Japan correspond well with the CO-enhanced events over the same region shown in Fig. 7.
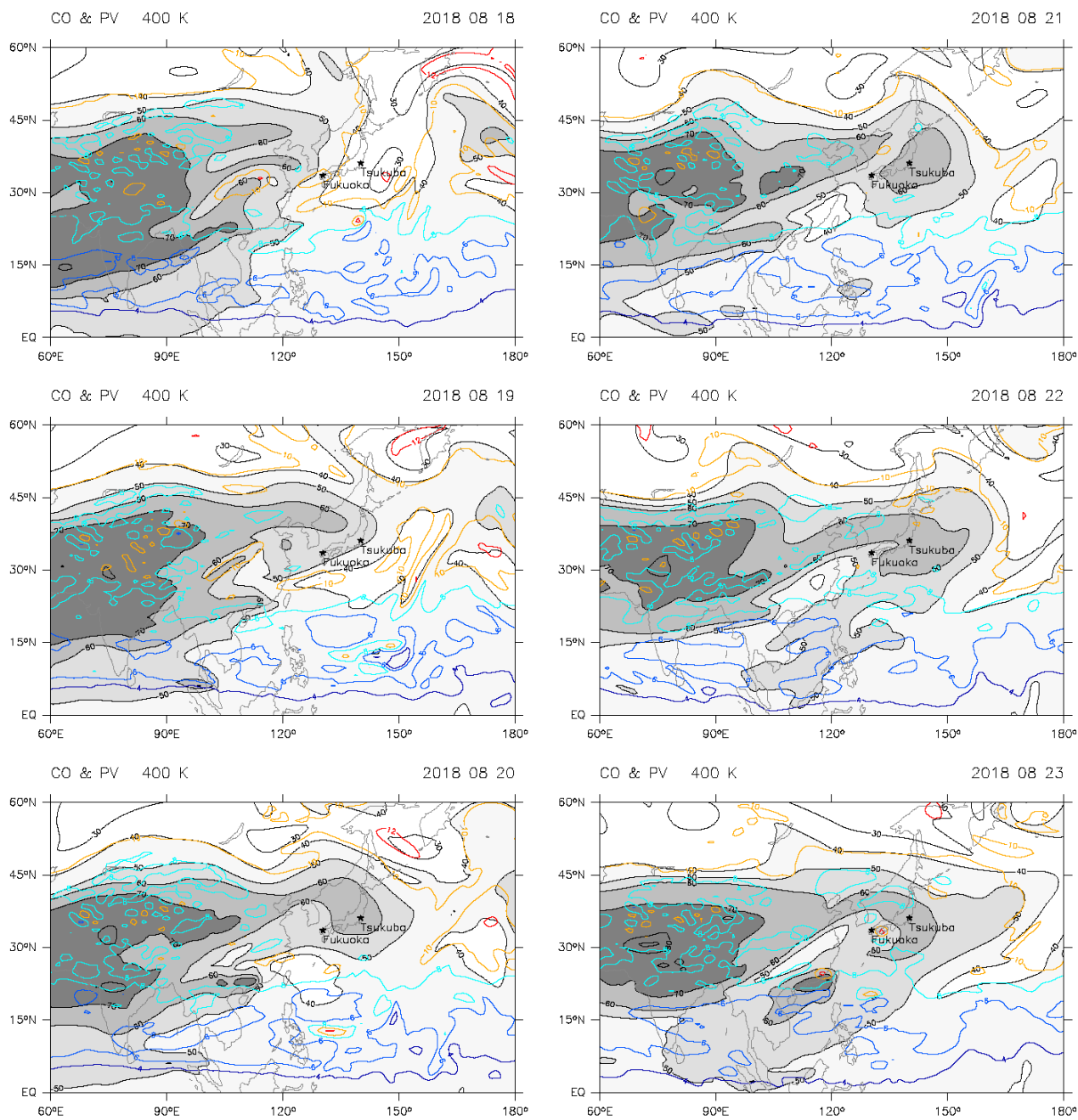
Figure 6 Horizontal distribution of daily averaged CO (black contours with grey tone, with intervals of 10 ppbv) and potential vorticity (PV; coloured contours at intervals of 2 PV Unit where 1 PV Unit equals to 10^{-6} K m^2 kg^{-1} s^{-1}) at the 400 K potential-temperature level during 18–23 August 2018 (dates indicated at top right of each plot), using CAMS reanalysis data.

250
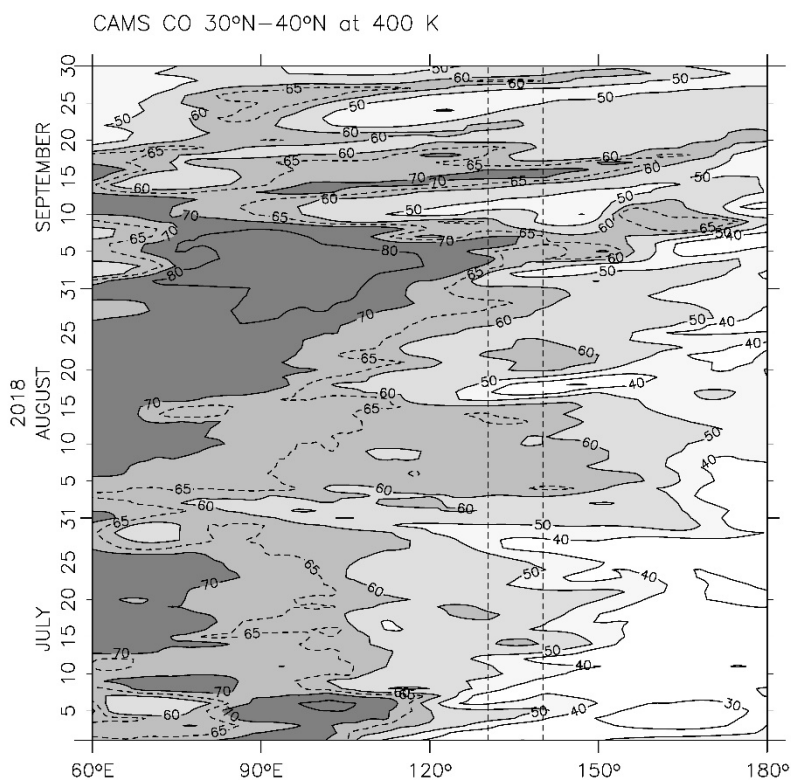
Figure 7 Longitude–time distribution of daily averaged CO concentration at 400 K potential temperature averaged over 30°N–40°N, using
255   CAMS reanalysis data. The contour interval is 10 ppbv, with 65 ppbv contours added (dotted). Vertical dotted lines indicate the locations of
the two lidar sites, Fukuoka and Tsukuba.
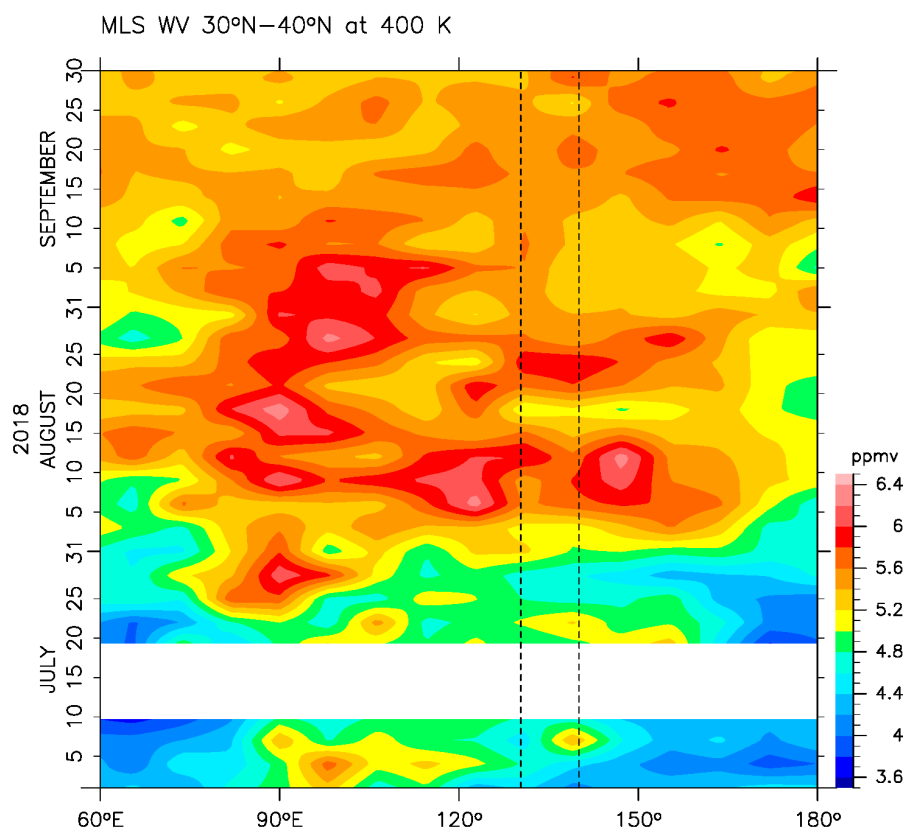
260

Figure 8 As for Fig. 7, but for water vapour (in ppmv) at 400 K measured with the satellite MLS instrument. Data for the 30°N–40°N region have been aggregated into 3-day and 8°-longitude bins, each constituting about 10 individual data points. The white region indicates missing measurements.

265

3.3 Satellite aerosol data

Lidar is sensitive to various types of volcanic aerosol (e.g., Yasui et al., 1996; Sakai et al., 2016; Khaykin et al., 2017). The lower stratosphere is continuously influenced by volcanic eruptions (GVP, 2013), which inject various types of particle and gas into the atmosphere (e.g., Robock, 2000). Among them, solid ash particles may remain in the stratosphere for up to a few

270   months, while liquid H_2SO_4 particles resulting from reaction of volcanic SO_2 and H_2S gases with OH and H_2O may remain for a year or more. Aerosol particles are also emitted from biomass burning and forest fires and, although these particles rarely reach the stratosphere, extensive fire events can influence the stratospheric aerosol loading (e.g., Khaykin et al., 2018; Peterson et al., 2018). In this section, the global lower-stratospheric aerosol loading during the summer of 2018 is investigated by the analysis of satellite aerosol data.

275

The time–latitude distribution of zonal-mean lower-stratospheric aerosol optical depth (AOD) at 675 nm from the OMPS LP satellite instrument is shown in Figure 9. At high NH latitudes, the lower-stratospheric AOD increased in the summer of 2017 due to extensive wildfires in Canada (Khaykin et al., 2018; Peterson et al., 2018), but their influence was negligible by early 2018. In July 2018, the eruption of Ambae (Aoba; 15.389°S, 167.835°E; GVP, 2019), Vanuatu, in the tropical western Pacific,

280   caused increasing stratospheric AOD in the tropics. We also observed very weak signals around the same latitude from the beginning of April 2018, possibly due to the eruption of the same Ambae during March–April 2018 (GVP, 2018). However, the lower stratospheric AOD at 25°N–40°N was relatively low during July–September 2018, at least on a zonal-mean scale. The monthly mean CALIOP attenuated scattering-ratio distribution due to aerosol particles at 17 km in July and August 2018 is shown in Figure 10 where the ATAL is evident, with enhanced aerosol signals over the ASM region. In August there was

285   also a hint of eastward extension of the ATAL to Japan, with a slight increase in the scattering ratio. By August, effects of the Ambae eruption had extended to about half of the tropics, but not have reached Japan directly (see also the 10-day backward trajectories; Figs. 4 and 5). In summary, enhanced aerosol particle signals observed at Tsukuba (36.1°N) and Fukuoka (33.55°N) were thus unlikely due to volcanic eruptions or northern wildfires.

290
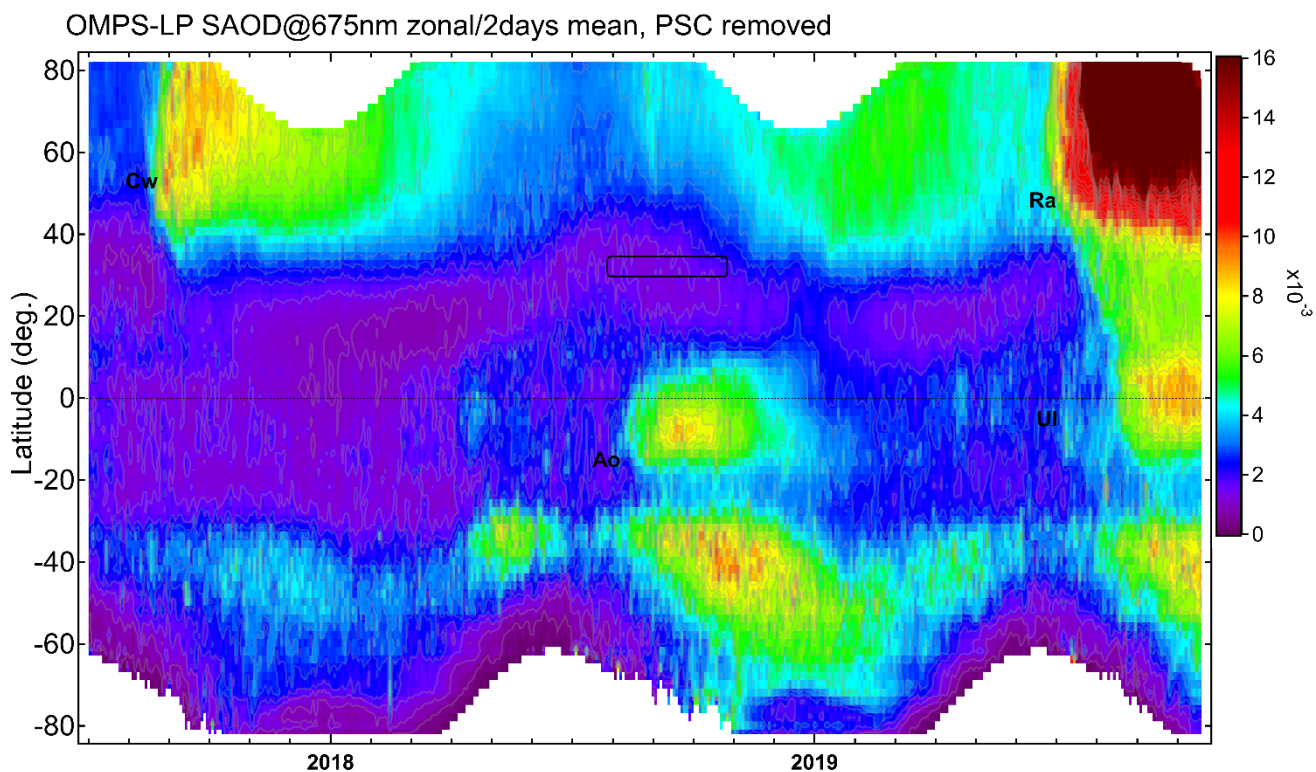
Figure 9 Time–latitude distribution of zonal- and 2-day-mean lower-stratospheric aerosol optical depth at 675 nm between the tropopause and 21 km altitude, from July 2017 to October 2019, as calculated from OMPS LP satellite data. The tropopause altitude for each OMPS LP profile was provided within the OMPS LP dataset. Signals due to Polar Stratospheric Clouds (PSCs) have been removed. Major events that significantly enhanced NH stratospheric aerosol loading are labelled: Cw, Canadian wildfires in the summer of 2017; Ao, Ambae (Aoba) eruption, Vanuatu (July 2018); Ra, Raikoke eruption, Kuril Islands, Russia (June 2019); Ul, Ulawun eruption, Papua New Guinea (July, August, and October 2019) (GVP, 2013). Rectangular box indicates the period and location of the lidar measurements; white regions indicate missing measurements.

300
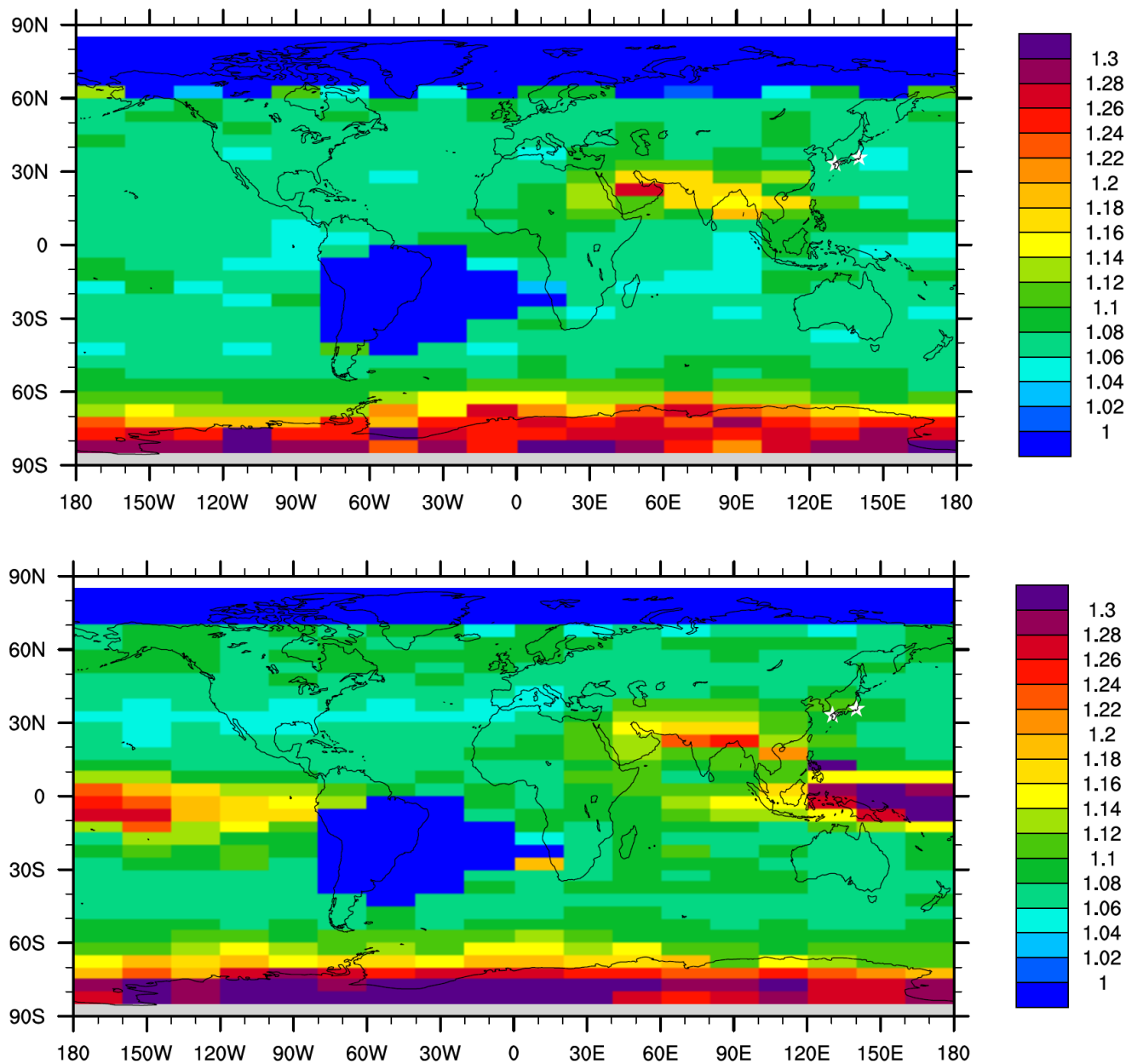
305 **Figure 10** Monthly mean horizontal distribution of attenuated scattering ratio at 17.042 km observed with the CALIOP satellite instrument in (top) July 2018 and (bottom) August 2018. Spatial bins are 5° in latitude, 20° in longitude, and 900 m in altitude. Clouds and PSCs have been removed (Sect. 2.2). The two lidar station locations are marked with white stars.

4 Summary and conclusions

Lidar aerosol-particle measurements at Tsukuba and Fukuoka, Japan, during the summer of 2018, were investigated to determine whether these lidars are capable of detecting the eastward extension of the ATAL from the ASM anticyclone in the UTLS. Both lidars observed enhanced aerosol-particle signals between the local tropopause and up to a few km above it, with the BSR values of ~1.10 (1.07–1.18) and PDR values of ~5% (3%–10%) at Tsukuba and with similar BSR but lower PDR values at Fukuoka. The PDR difference between the two sites may be due to the Fukuoka lidar operating on only 11 nights during the three-month period. The lidars often detected strong signals (BSR values of >1.25 and with PDR values >>10%) due to ice cirrus clouds below the tropopause. The Tsukuba measurements indicated that timescales of lower-stratospheric enhancements are of a few days. Backward trajectory calculations and reanalysis CO data support the hypothesis that airmasses with enhanced aerosol signals originate in the ASM anticyclone in association with eastward shedding vortices. OMPS LP and CALIOP satellite data indicated that the 25°N–40°N region was not influenced by volcanic eruptions and extensive biomass burning events during July–September 2018. Our results indicate that the enhanced aerosol particle levels measured at Tsukuba and Fukuoka are due to eastward shedding vortices of the ATAL from the ASM anticyclone; i.e., they originated from pollutants emitted from Asian countries and transported vertically by convection in the ASM region.

It is also noted that the "westward" extension of the ATAL to northern midlatitudes was reported by Khaykin et al. (2017), based on ground-based lidar at the Observatoire de Haute-Provence (OHP) in southern France (43.9°N, 5.7°E), with a layer of enhanced aerosol in the lower stratosphere with an average BSR value of 1.05 being a systematic feature during August–October. This aerosol layer was shown to correlate with the seasonal water-vapour maximum, suggesting the influx of convectively moistened air from the ASM anticyclone, whose influence on the extratropical lower stratosphere in late summer to early winter is well known (e.g., Vogel et al., 2014; Müller et al., 2016; Rolf et al., 2018).

The PDR values obtained at Tsukuba, i.e., ~5% (3%–10%) suggest that these enhanced particles are solid particles, rather than spherical, liquid H_2SO_4 particles (PDR ~0%) or cirrus ice particles (PDR > 25%–30%). The observed values may be consistent with those of solid NH_4NO_3 particles recently suggested by Höpfner et al. (2019). There seem to have been no previous studies of lidar PDR values for solid NH_4NO_3 particles. Sakai et al. (2010) investigated PDR values of other particle types in laboratory experiments; among these particles, sub-micrometre sea-salt and ammonium sulphate crystals (e.g., Plate 9 (pages 237–239) of Pruppacher and Klett, 1997) were found to have PDR values of ~8% PDR and ~4% PDR, respectively. Solid NH_4NO_3 particles may have similar PDR values as their crystal structures could be similar. Small non-zero PDR values can occur if enhanced liquid H_2SO_4 particles and fresh ash particles from volcanic eruptions are mixed, although satellite data indicate this is less plausible (Sect. 3.3). Lidar measurements at Mauna Loa, Hawaii, indicated no signals from volcanic eruptions during the summer of 2018 (Chouza et al., 2020). Also, at the OHP lidar site in France, any enhancement in the lower stratospheric aerosol abundance was observed during the summer of 2018.

Lower-stratospheric aerosol enhancement over Japan was observed mainly during August–September, and seldom in July.
345 This may be partly explained by the seasonality of the concentration of solid NH_4NO_3 particles in the ASM anticyclone (Höpfner et al., 2019), peaking in August with significant year-to-year variations. Furthermore, June and July are in the rainy season for most of Japan, in association with the "Baiu" frontal system (e.g., Ninomiya and Shibagaki, 2007). In July 2018, severe rainfall and flood events occurred early in the month (Shimpo et al., 2019), after which many parts of Japan experienced high surface temperatures with cumulonimbus clouds in several areas. Typhoons, synoptic low systems, and frontal systems
350 affected Japan through to the end of September 2018, with these rainfall and thick-cloud events preventing the lidars from sensing the lower stratosphere, causing many of the missed-data slots in Fig. 1.

In summary, part of the ATAL in the ASM anticyclone airmass is transported eastward and passes over Japan in the UTLS. Lidars in Japan can observe the lower stratospheric portion of these aerosol particles if conditions permit, with summer-time
355 active convection and various weather systems often preventing their sensing of the lower stratosphere. Volcanic eruptions and extensive wildfires may complicate the detection of particles of ATAL origin over Japan. The upper tropospheric portion of these particles is either depleted by tropospheric processes (convection and wet scavenging) or obscured by much stronger cirrus-cloud signals. Despite the limited sampling, the lidar detection of ATAL particles verifies eastward UTLS transport associated with sub-seasonal-scale dynamics of the ASM anticyclone, a process observed by satellite instruments and predicted
360 by models. The spatial extent, and chemical and aerosol content of this transport process is the main focus of an upcoming airborne field campaign, the Asian summer monsoon Chemical and Climate Impact Project (ACCLIP; Pan et al., 2019), which is scheduled to take place over the western Pacific during July–August 2021.

365 **Appendix A**

The time–height distribution of TDR at Tsukuba is shown in Figure A1, complementing Fig. 1b (PDR distribution).
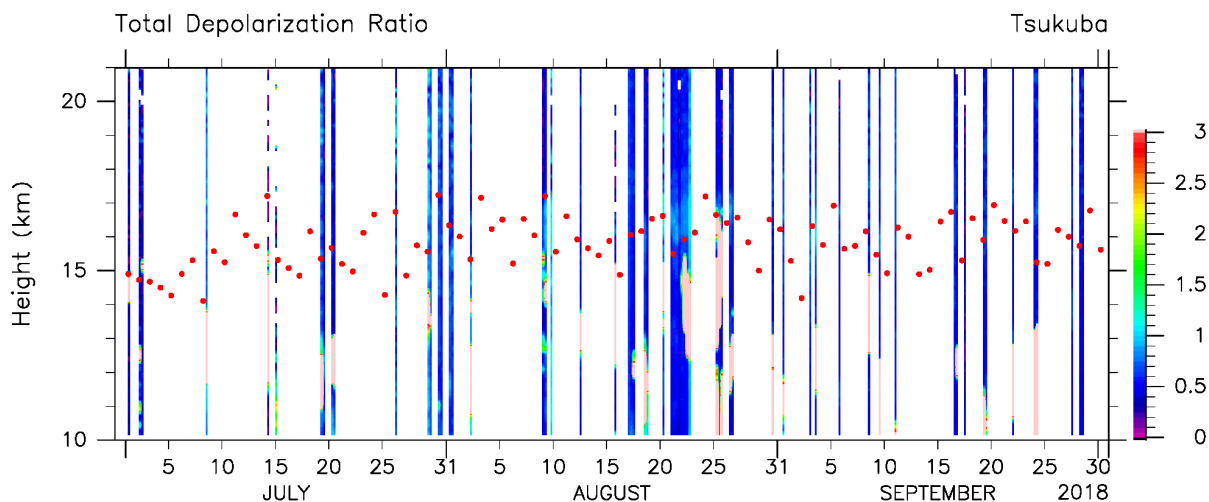
Figure A1 As for Fig. 1, but for the total depolarization ratio (TDR, %).

370

Data availability

Lidar data analysed in this study can be downloaded from the following websites: https://mri-2.mri-jma.go.jp/owncloud/s/GrNGNiGKzq8tjqH for Tsukuba; and https://www.cis.fukuoka-u.ac.jp/~ksiraisi/LidarDataArchive/Fukuoka_2018summer.zip for Fukuoka. ERA5 and CAMS data can be downloaded from the Copernicus website, with the former from https://cds.climate.copernicus.eu and the latter from https://ads.atmosphere.copernicus.eu. MLS Version 4.2 Level 2 data can be downloaded from https://acdisc.gesdisc.eosdis.nasa.gov/data/Aura_MLS_Level2/. OMPS LP Level 2 Version 1.5 data can be downloaded from https://snpp-omps.gesdisc.eosdis.nasa.gov/data. CALIOP data can be downloaded from https://asdc.larc.nasa.gov/search.

380

Author contributions

MF, MS, and LLP designed the study. MF, T Sakai, and KS analysed lidar data and drafted the manuscript. YI calculated trajectories. MF and HX analysed CAMS data. SK analysed MLS and OMPS LP data, while T Shibata analysed CALIOP data. All authors contributed to the interpretation, and reviewed and edited the manuscript.

385

Competing interests

The authors declare that they have no conflict of interest.

Acknowledgements

390   This study was financially supported by the research grant for Mission Research on Sustainable Humanosphere from Research Institute for Sustainable Humanosphere (RISH), Kyoto University, Japan, for the fiscal years 2019–2020. The GFD-DENNOU library was used for producing Figures 1–7 and A1. We thank Nawo Eguchi and Suginori Iwasaki for valuable comments on draft manuscript.

395   ## *Financial support*

This study was financially supported by the research grant for Mission Research on Sustainable Humanosphere from Research Institute for Sustainable Humanosphere (RISH), Kyoto University, Japan for the fiscal years 2019–2020.

References

400   Adachi, H., Shibata, T., Iwasaka, Y., and Fujiwara, M.: Calibration method for the lidar-observed stratospheric depolarization ratio in the presence of liquid aerosol particles, Appl. Opt., 40(36), 6587–6595, https://doi.org/10.1364/AO.40.006587, 2001.

Amemiya, A., and Sato, K.: A two-dimensional dynamical model for the subseasonal variability of the Asian monsoon anticyclone, J. Atmos. Sci., 75, 3597–3612, https://doi.org/10.1175/JAS-D-17-0208.1, 2018.

Bossolasco, A., Jegou, F., Sellitto, P., Berthet, G., Kloss, C., and Legras, B.: Global modelling studies of composition and
405   decadal trends of the Asian Tropopause Aerosol Layer, Atmos. Chem. Phys. Discuss., https://doi.org/10.5194/acp-2020-677, in review, 2020.

Brunamonti, S., Jorge, T., Oelsner, P., Hanumanthu, S., Singh, B. B., Kumar, K. R., Sonbawne, S., Meier, S., Singh, D., Wienhold, F. G., Luo, B. P., Boettcher, M., Poltera, Y., Jauhiainen, H., Kayastha, R., Karmacharya, J., Dirksen, R., Naja, M., Rex, M., Fadnavis, S., and Peter, T.: Balloon-borne measurements of temperature, water vapor, ozone and aerosol
410   backscatter on the southern slopes of the Himalayas during StratoClim 2016–2017, Atmos. Chem. Phys., 18, 15937–15957, https://doi.org/10.5194/acp-18-15937-2018, 2018.

Chen, Z., Bhartia, P. K., Loughman, R., Colarco, P., and DeLand, M.: Improvement of stratospheric aerosol extinction retrieval from OMPS/LP using a new aerosol model, Atmos. Meas. Tech., 11, 6495–6509, https://doi.org/10.5194/amt-11-6495-2018, 2018.

415 Chouza, F., Leblanc, T., Barnes, J., Brewer, M., Wang, P., and Koon, D.: Long-term (1999–2019) variability of stratospheric aerosol over Mauna Loa, Hawaii, as seen by two co-located lidars and satellite measurements, Atmos. Chem. Phys., 20, 6821–6839, https://doi.org/10.5194/acp-20-6821-2020, 2020.

Enomoto, T., Hoskins, B. J., and Matsuda, Y.: The formation mechanism of the Bonin high in August. Quart. J. Roy. Meteorol. Soc., 129, 157–178, https://doi.org/10.1256/qj.01.211, 2003.

420 Fadnavis, S., Roy, C., Chattopadhyay, R., Sioris, C. E., Rap, A., Müller, R., Kumar, K. R., and Krishnan, R.: Transport of trace gases via eddy shedding from the Asian summer monsoon anticyclone and associated impacts on ozone heating rates, Atmos. Chem. Phys., 18, 11493–11506, https://doi.org/10.5194/acp-18-11493-2018, 2018.

Fujiwara, M., Iwasaki, S., Shimizu, A., Inai, Y., Shiotani, M., Hasebe, F., Matsui, I., Sugimoto, N., Okamoto, H., Nishi, N., Hamada, A., Sakazaki, T., and Yoneyama, K.: Cirrus observations in the tropical tropopause layer over the western Pacific, 425 J. Geophys. Res., 114(D9), D09304, https://doi.org/10.1029/2008JD011040, 2009.

GVP (Global Volcanism Program): Volcanoes of the World, v. 4.9.0 (04 Jun 2020), Venzke, E (ed.), Smithsonian Institution, https://doi.org/10.5479/si.GVP.VOTW4-2013, 2013 (last accessed: 3 July 2020).

GVP (Global Volcanism Program): Report on Ambae (Vanuatu) (Crafford, A.E., and Venzke, E., eds.), Bulletin of the Global Volcanism Network, 43:7, Smithsonian Institution, https://doi.org/10.5479/si.GVP.BGVN201807-257030, 2018 (last 430 accessed: 4 July 2020).

GVP (Global Volcanism Program): Report on Ambae (Vanuatu) (Krippner, J.B., and Venzke, E., eds.), Bulletin of the Global Volcanism Network, 44:2, Smithsonian Institution, https://doi.org/10.5479/si.GVP.BGVN201902-257030, 2019 (last accessed: 4 July 2020).

Haarig, M., Ansmann, A., Baars, H., Jimenez, C., Veselovskii, I., Engelmann, R., and Althausen, D.: Depolarization and lidar 435 ratios at 355, 532, and 1064 nm and microphysical properties of aged tropospheric and stratospheric Canadian wildfire smoke, Atmos. Chem. Phys., 18, 11847–11861, https://doi.org/10.5194/acp-18-11847-2018, 2018.

Hanumanthu, S., Vogel, B., Müller, R., Brunamonti, S., Fadnavis, S., Li, D., Ölsner, P., Naja, M., Singh, B. B., Kumar, K. R., Sonbawne, S., Jauhiainen, H., Vömel, H., Luo, B., Jorge, T., Wienhold, F. G., Dirkson, R., and Peter, T.: Strong variability of the Asian Tropopause Aerosol Layer (ATAL) in August 2016 at the Himalayan foothills, Atmos. Chem. Phys. Discuss., 440 https://doi.org/10.5194/acp-2020-552, in review, 2020.

Hersbach, H., Bell, B., Berrisford, P., Hirahara, S., Horányi, A., Muñoz-Sabater, J., Nicolas, J., Peubey, C., Radu, R., Schepers, D., Simmons, A., Soci, C., Abdalla, S., Abellan, X., Balsamo, G., Bechtold, P., Biavati, G., Bidlot, J., Bonavita, M., Chiara, G., Dahlgren, P., Dee, D., Diamantakis, M., Dragani, R., Flemming, J., Forbes, R., Fuentes, M., Geer, A., Haimberger, L., Healy, S., Hogan, R. J., Hólm, E., Janisková, M., Keeley, S., Laloyaux, P., Lopez, P., Lupu, C., Radnoti, G., Rosnay, P.,

445   Rozum, I., Vamborg, F., Villaume, S., and Thépaut, J.: The ERA5 global reanalysis, Quart. J. Royal Meteorol. Soc., in press, https://doi.org/10.1002/qj.3803, 2020.

Honomichl, S. B., and Pan, L. L.: Transport from the Asian summer monsoon anticyclone over the western Pacific, J. Geophys. Res. Atmos., in press, https://doi.org/10.1029/2019JD032094, 2020.

Höpfner, M., Ungermann, J., Borrmann, S., Wagner, R., Spang, R., Riese, M., Stiller, G., Appel, O., Batenburg, A. M., Bucci,

450   S., Cairo, F., Dragoneas, A., Friedl-Vallon, F., Hünig, A., Johansson, S., Krasauskas, L., Legras, B., Leisner, T., Mahnke, C., Möhler, O., Molleker, S., Müller, R., Neubert, T., Orphal, J., Preusse, P., Rex, M., Saathoff, H., Stroh, F., Weigel, R., and Wohltmann, I.: Ammonium nitrate particles formed in upper troposphere from ground ammonia sources during Asian monsoons, Nat. Geosci., 12(8), 608–612, https://doi.org/10.1038/s41561-019-0385-8, 2019.

Inai, Y.: Long-term variation in the mixing fraction of tropospheric and stratospheric air masses in the upper tropical

455   tropopause layer, J. Geophys. Res. Atmos., 123, 4890–4909, https://doi.org/10.1029/2018JD028300, 2018.

Inai, Y., Aoki, S., Honda, H., Furutani, H., Matsumi, Y., Ouchi, M., Sugawara, S., Hasebe, F., Uematsu, M., and Fujiwara, M.: Balloon-borne tropospheric CO_2 observations over the equatorial eastern and western Pacific, Atmos. Environ., 184, 24–36, https://doi.org/10.1016/j.atmosenv.2018.04.016, 2018.

Inness, A., Ades, M., Agustí-Panareda, A., Barré, J., Benedictow, A., Blechschmidt, A.-M., Dominguez, J. J., Engelen, R.,

460   Eskes, H., Flemming, J., Huijnen, V., Jones, L., Kipling, Z., Massart, S., Parrington, M., Peuch, V.-H., Razinger, M., Remy, S., Schulz, M., and Suttie, M.: The CAMS reanalysis of atmospheric composition, Atmos. Chem. Phys., 19, 3515–3556, https://doi.org/10.5194/acp-19-3515-2019, 2019.

Khaykin, S. M., Godin-Beekmann, S., Keckhut, P., Hauchecorne, A., Jumelet, J., Vernier, J.-P., Bourassa, A., Degenstein, D. A., Rieger, L. A., Bingen, C., Vanhellemont, F., Robert, C., DeLand, M., and Bhartia, P. K.: Variability and evolution of

465   the midlatitude stratospheric aerosol budget from 22 years of ground-based lidar and satellite observations, Atmos. Chem. Phys., 17, 1829–1845, https://doi.org/10.5194/acp-17-1829-2017, 2017.

Khaykin, S. M., Godin-Beekmann, S., Hauchecorne, A., Pelon, J., Ravetta, F., and Keckhut, P.: Stratospheric smoke with unprecedentedly high backscatter observed by lidars above southern France, Geophys. Res. Lett., 45(3), 1639–1646, https://doi.org/10.1002/2017GL076763, 2018.

470 Livesey, N. J., Read, W. G., Wagner, P. A., Froidevaux, L., Lambert, A., Manney, G. L., Millán Valle, L. F., Pumphrey, H. C., Santee, M. L., Schwartz, M. J., Wang, S., Fuller, R. A., Jarnot, R. F., Knosp, B. W., Martinez, E., and Lay, R. R.: Aura Microwave Limb Sounder (MLS) Version 4.2x Level 2 and 3 data quality and description document, Tech. Rep. JPL D-33509 Rev. E, available at: https://mls.jpl.nasa.gov/ (last accessed: 26 August 2020).

Luo, J., Pan, L. L., Honomichl, S. B., Bergman, J. W., Randel, W. J., Francis, G., Clerbaux, C., George, M., Liu, X., and Tian,

475   W.: Space–time variability in UTLS chemical distribution in the Asian summer monsoon viewed by limb and nadir satellite sensors, Atmos. Chem. Phys., 18, 12511–12530, https://doi.org/10.5194/acp-18-12511-2018, 2018.

Müller, S., Hoor, P., Bozem, H., Gute, E., Vogel, B., Zahn, A., Bönisch, H., Keber, T., Krämer, M., Rolf, C., Riese, M., Schlager, H., and Engel, A.: Impact of the Asian monsoon on the extratropical lower stratosphere: trace gas observations

during TACTS over Europe 2012, Atmos. Chem. Phys., 16, 10573–10589, https://doi.org/10.5194/acp-16-10573-2016, 2016.

Ninomiya, K., and Shibagaki, Y.: Multi-scale features of the Meiyu-Baiu front and associated precipitation systems, J. Meteorol. Soc. Japan, 85B, 103–122, https://doi.org/10.2151/jmsj.85B.103, 2007.

Pan, L. L., Honomichl, S. B., Kinnison, D. E., Abalos, M., Randel, W. J., Bergman, J. W., and Bian, J.: Transport of chemical tracers from the boundary layer to stratosphere associated with the dynamics of the Asian summer monsoon, J. Geophys. Res. Atmos., 121, 14,159–14,174, https://doi.org/10.1002/2016JD025616, 2016.

Pan, L., Kinnison, D., Liang, Q., Atlas, E., Bresch, J. Case, P., Fujiwara, M., Honomichl, S., Lait, L., Newman, P., Nishi, N., Randel, B., Smith, R., Tilmes, S., and Toon, B.: Progress in the Asian summer monsoon Chemical and Climate Impact Project (ACCLIP), presented at the AGU Fall Meeting 2019, American Geophysical Union, San Francisco, CA, USA, Abstract No. A51K-2788, https://agu.confex.com/agu/fm19/meetingapp.cgi/Paper/543867, 2019 (last accessed: 11 October 2020). (Poster pdf available at http://n2t.net/ark:/85065/d7m3301b, last accessed: 11 October 2020.)

Peterson, D. A., Campbell, J. R., Hyer, E. J., Fromm, M. D., Kablick, G. P., III, Cossuth, J. H., and DeLand, M. T.: Wildfire-driven thunderstorms cause a volcano-like stratospheric injection of smoke, npj Clim. Atmos. Sci., 1(1), https://doi.org/10.1038/s41612-018-0039-3, 2018.

Popovic, J. M., and Plumb, R. A.: Eddy shedding from the upper-tropospheric Asian monsoon anticyclone, J. Atmos. Sci., 58, 93–104, https://doi.org/10.1175/1520-0469(2001)058<0093:ESFTUT>2.0.CO;2, 2001.

Prata, A. T., Young, S. A., Siems, S. T., and Manton, M. J.: Lidar ratios of stratospheric volcanic ash and sulfate aerosols retrieved from CALIOP measurements, Atmos. Chem. Phys., 17, 8599–8618, https://doi.org/10.5194/acp-17-8599-2017, 2017.

Pruppacher, H. R., and Klett, J. D.: Microphysics and Clouds and Precipitation, Second Revised and Enlarged Edition, Kluwer Academic Pub., Dordrecht, 954 pp., 1996.

Randel, W. J., Park, M., Emmons, L., Kinnison, D., Bernath, P., Walker, K. A., Boone, C., and Pumphrey, H.: Asian monsoon transport of pollution to the stratosphere, Science, 328 (5978), 611–613, https://doi.org/10.1126/science.1182274, 2010.

Randel, W. J., Zhang, K., and Fu, R.: What controls stratospheric water vapor in the NH summer monsoon regions?, J. Geophys. Res. Atmos., 120, 7988–8001, https://doi.org/10.1002/2015JD023622, 2015.

Robock, A.: Volcanic eruptions and climate, Rev. Geophys., 38, 191–219, https://doi.org/10.1029/1998RG000054, 2000.

Rolf, C., Vogel, B., Hoor, P., Afchine, A., Günther, G., Krämer, M., Müller, R., Müller, S., Spelten, N., and Riese, M.: Water vapor increase in the lower stratosphere of the Northern Hemisphere due to the Asian monsoon anticyclone observed during the TACTS/ESMVal campaigns, Atmos. Chem. Phys., 18, 2973–2983, https://doi.org/10.5194/acp-18-2973-2018, 2018.

Sakai, T., Nagai, T., Nakazato, M., Mano, Y., and Matsumura, T.: Ice clouds and Asian dust studied with lidar measurements of particle extinction-to-backscatter ratio, particle depolarization, and water-vapor mixing ratio over Tsukuba, Appl. Opt., 42, 7103-7116, https://doi.org/10.1364/AO.42.007103, 2003.

Sakai, T., Nagai, T., Zaizen, Y., and Mano, Y.: Backscattering linear depolarization ratio measurements of mineral, sea-salt, and ammonium sulfate particles simulated in a laboratory chamber, Appl. Opt., 49(23), 4441–4449, https://doi.org/10.1364/AO.49.004441, 2010.

Sakai, T., Uchino, O., Nagai, T., Liley, B., Morino, I., and Fujimoto, T.: Long-term variation of stratospheric aerosols observed with lidars over Tsukuba, Japan, from 1982 and Lauder, New Zealand, from 1992 to 2015, J. Geophys. Res. Atmos., 121, 10,283–10,293, https://doi.org/10.1002/2016JD025132, 2016.

Santee, M. L., Manney, G. L., Livesey, N. J., Schwartz, M. J., Neu, J. L., and Read, W. G.: A comprehensive overview of the climatological composition of the Asian summer monsoon anticyclone based on 10 years of Aura Microwave Limb Sounder measurements, J. Geophys. Res. Atmos., 122, 5491–5514, https://doi.org/10.1002/2016JD026408, 2017.

Shimpo, A., Takemura, K., Wakamatsu, S., Togawa, H., Mochizuki, Y., Takekawa, M., Tanaka, S., Yamashita, K., Maeda, S., Kurora, R., Murai, H., Kitabatake, N., Tsuguti, H., Mukougawa, H., Iwasaki, T., Kawamura, R., Kimoto, M., Takayabu, I., Takayabu, Y.N., Tanimoto, Y., Hirooka, T., Masumoto, Y., Watanabe, M., Tsuboki, K., and Nakamura, H.: Primary Factors behind the Heavy Rain Event of July 2018 and the subsequent heat wave in Japan, Sci. Online Lett. Atmos., 15A, 13–18, https://doi.org/10.2151/sola.15A-003, 2019.

Thomason, L. W., Pitts, M. C., and Winker, D. M.: CALIPSO observations of stratospheric aerosols: a preliminary assessment, Atmos. Chem. Phys., 7, 5283–5290, https://doi.org/10.5194/acp-7-5283-2007, 2007.

Uchino, O., Nagai, T., Fujimoto, T., Fujiwara, M., Akiyoshi, H., Yasumatsu, S., Hayashida, S., Sasano, Y., Nakane, H., Iwasaka, Y., Hase, M., Shibata, T., Itabe, T., Asai, K., Nomura, A., Saito, Y., Kano, T., Sai, Y., Tamaki, K., Nomura, R., Sunagawa, T., Nagasawa, C., Abo, M., Idesako, Y., and Kai, K.: Observation of the Pinatubo volcanic cloud by lidar network in Japan, J. Meteorol. Soc. Jpn., 71, 285–296, https://doi.org/10.2151/jmsj1965.71.2_285, 1993.

Ungermann, J., Ern, M., Kaufmann, M., Müller, R., Spang, R., Ploeger, F., Vogel, B., and Riese, M.: Observations of PAN and its confinement in the Asian summer monsoon anticyclone in high spatial resolution, Atmos. Chem. Phys., 16, 8389–8403, https://doi.org/10.5194/acp-16-8389-2016, 2016.

Vernier, J.-P., Fairlie, T. D., Natarajan, M., Wienhold, F. G., Bian, J., Martinsson, B. G., Crumeyrolle, S., Thomason, L. W., and Bedka, K. M.: Increase in upper tropospheric and lower stratospheric aerosol levels and its potential connection with Asian pollution, J. Geophys. Res. Atmos., 120, 1608–1619, https://doi.org/10.1002/2014JD022372, 2015.

Vernier, J.-P., Fairlie, T. D., Deshler, T., Venkat Ratnam, M., Gadhavi, H., Kumar, B. S., Natarajan, M., Pandit, A. K., Akhil Raj, S. T., Hemanth Kumar, A., Jayaraman, A., Singh, A. K., Rastogi, N., Sinha, P. R., Kumar, S., Tiwari, S., Wegner, T., Baker, N., Vignelles, D., Stenchikov, G., Shevchenko, I., Smith, J., Bedka, K., Kesarkar, A., Singh, V., Bhate, J., Ravikiran, V., Durga Rao, M., Ravindrababu, S., Patel, A., Vernier, H., Wienhold, F. G., Liu, H., Knepp, T. N., Thomason, L., Crawford, J., Ziemba, L., Moore, J., Crumeyrolle, S., Williamson, M., Berthet, G., Jégou, F., and Renard, J.-B.: BATAL: The Balloon measurement campaigns of the Asian Tropopause Aerosol Layer, Bull. Amer. Meteorol. Soc., 99(5), 955–973, 2018.

Vogel, B., Günther, G., Müller, R., Grooß, J.-U., Hoor, P., Krämer, M., Müller, S., Zahn, A., and Riese, M.: Fast transport
545   from Southeast Asia boundary layer sources to northern Europe: rapid uplift in typhoons and eastward eddy shedding of the
    Asian monsoon anticyclone, Atmos. Chem. Phys., 14, 12745–12762, https://doi.org/10.5194/acp-14-12745-2014, 2014.

Vogel, B., Günther, G., Müller, R., Grooß, J.-U., Afchine, A., Bozem, H., Hoor, P., Krämer, M., Müller, S., Riese, M., Rolf,
    C., Spelten, N., Stiller, G. P., Ungermann, J., and Zahn, A.: Long-range transport pathways of tropospheric source gases
    originating in Asia into the northern lower stratosphere during the Asian monsoon season 2012, Atmos. Chem. Phys., 16,
550   15301–15325, https://doi.org/10.5194/acp-16-15301-2016, 2016.

Winker, D. M., Hunt, W. H., and McGill, M. J.: Initial performance assessment of CALIOP, Geophys. Res.Lett., 34(19),
    L19803, https://doi.org/10.1029/2007GL030135, 2007.

Winker, D. M., Pelon, J., Coakley, J. A., Jr., Ackerman, S. A., Charlson, R. J., Colarco, P. R., Flamant, P., Fu, Q., Hoff, R. M.,
    Kittaka, C., Kubar, T. L., Le Treut, H., Mccormick, M. P., Mégie, G., Poole, L., Powell, K., Trepte, C., Vaughan, M. A.,
555   and Wielicki, B. A.: The CALIPSO mission: A global 3D view of aerosols and clouds, Bull. Amer. Meteorol. Soc., 91(9),
    1211–1230, https://doi.org/10.1175/2010BAMS3009.1, 2010.

Yasui, M., Fujiwara, M., Akiyoshi, H., Ikawa, S., Nonaka, H., Shiraishi, K.: Seasonal variation of Pinatubo volcanic aerosols
    in the stratosphere observed by lidar in Fukuoka, J. Geomag. Geoelectr., 47, 989-998, https://doi.org/10.5636/jgg.47.989,
    1995.

560 Yasui, M, Fujiwara, M., Shibata, T., Akiyoshi, H., Ikawa, S., Shiraishi, K., Nonaka, H.: Variations of volcanic aerosols
    observed in Fukuoka - A comparison of Mt El Chichon and Mt Pinatubo events, J. Geomag., Geoelectr., 48, 403-413,
    https://doi.org/10.5636/jgg.48.403, 1996.